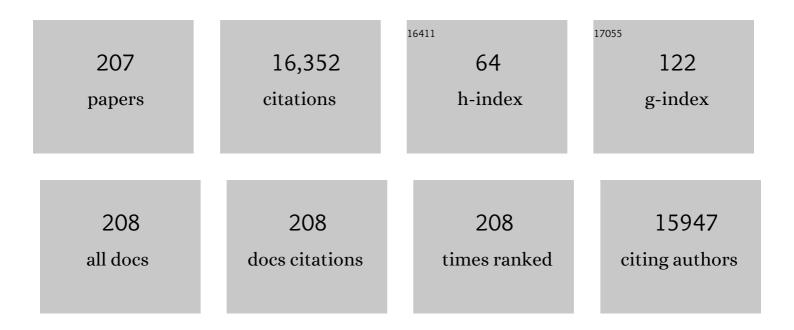
List of Publications by Year in descending order

Source: https://exaly.com/author-pdf/373517/publications.pdf Version: 2024-02-01



**RENUEL** 

#	Article	IF	CITATIONS
1	Recent Advances in Heterogeneous Photocatalytic CO <sub>2</sub> Conversion to Solar Fuels. ACS Catalysis, 2016, 6, 7485-7527.	5.5	1,035
2	Enhanced photocatalytic activity of g-C <sub>3</sub> N <sub>4</sub> for selective CO <sub>2</sub> reduction to CH <sub>3</sub> OH via facile coupling of ZnO: a direct Z-scheme mechanism. Journal of Materials Chemistry A, 2015, 3, 19936-19947.	5.2	812
3	Two Different Roles of Metallic Ag on Ag/AgX/BiOX (X = Cl, Br) Visible Light Photocatalysts: Surface Plasmon Resonance and Z-Scheme Bridge. ACS Catalysis, 2012, 2, 1677-1683.	5.5	768
4	Direct Z-scheme g-C3N4/WO3 photocatalyst with atomically defined junction for H2 production. Applied Catalysis B: Environmental, 2017, 219, 693-704.	10.8	617
5	Filling metal–organic framework mesopores with TiO2 for CO2 photoreduction. Nature, 2020, 586, 549-554.	13.7	554
6	Graphitic carbon nitride (g-C3N4)–Pt-TiO2 nanocomposite as an efficient photocatalyst for hydrogen production under visible light irradiation. Physical Chemistry Chemical Physics, 2012, 14, 16745.	1.3	479
7	Effect of graphitic carbon nitride microstructures on the activity and selectivity of photocatalytic CO2 reduction under visible light. Catalysis Science and Technology, 2013, 3, 1253.	2.1	441
8	Increasing visible-light absorption for photocatalysis with black BiOCl. Physical Chemistry Chemical Physics, 2012, 14, 82-85.	1.3	383
9	Recent advances in dye-sensitized semiconductor systems for photocatalytic hydrogen production. Journal of Materials Chemistry A, 2016, 4, 2365-2402.	5.2	368
10	Synthesis of Titanium Dioxide Nanoparticles with Mesoporous Anatase Wall and High Photocatalytic Activity. Journal of Physical Chemistry B, 2005, 109, 4947-4952.	1.2	359
11	Porous hypercrosslinked polymer-TiO2-graphene composite photocatalysts for visible-light-driven CO2 conversion. Nature Communications, 2019, 10, 676.	5.8	278
12	Highly Asymmetric Phthalocyanine as a Sensitizer of Graphitic Carbon Nitride for Extremely Efficient Photocatalytic H <sub>2</sub> Production under Near-Infrared Light. ACS Catalysis, 2014, 4, 162-170.	5.5	270
13	Synthesis of floriated ZnFe2O4 with porous nanorod structures and its photocatalytic hydrogen production under visible light. Journal of Materials Chemistry, 2010, 20, 3665.	6.7	252
14	Recent advances in the photocatalytic CO2 reduction over semiconductors. Catalysis Science and Technology, 2013, 3, 2481.	2.1	250
15	Synthesis of highly symmetrical BiOI single-crystal nanosheets and their {001} facet-dependent photoactivity. Journal of Materials Chemistry, 2011, 21, 12479.	6.7	223
16	Visible/Near-Infrared-Light-Induced H <sub>2</sub> Production over g-C <sub>3</sub> N <sub>4</sub> Co-sensitized by Organic Dye and Zinc Phthalocyanine Derivative. ACS Catalysis, 2015, 5, 504-510.	5.5	203
17	Enhanced Photocatalytic Hydrogen Production over Graphene Oxide–Cadmium Sulfide Nanocomposite under Visible Light Irradiation. Journal of Physical Chemistry C, 2012, 116, 22720-22726.	1.5	195
18	Template-Free Hydrothermal Synthesis of ZnIn <sub>2</sub> S <sub>4</sub> Floriated Microsphere as an Efficient Photocatalyst for H <sub>2</sub> Production under Visible-Light Irradiation. Journal of Physical Chemistry C, 2011, 115, 6149-6155.	1.5	184

#	Article	IF	CITATIONS
19	Preparation of AgIn <sub>5</sub> S <sub>8</sub> /TiO <sub>2</sub> Heterojunction Nanocomposite and Its Enhanced Photocatalytic H <sub>2</sub> Production Property under Visible Light. ACS Catalysis, 2013, 3, 170-177.	5.5	175
20	Photocatalytic hydrogen generation using a nanocomposite of multi-walled carbon nanotubes and TiO <sub>2</sub> nanoparticles under visible light irradiation. Nanotechnology, 2009, 20, 125603.	1.3	170
21	Electron-Donating or -Withdrawing Nature of Substituents Revealed by the Electrochemistry of Metal-Free Phthalocyanines. Inorganic Chemistry, 2006, 45, 2327-2334.	1.9	169
22	Effect of Annealing Temperature on the Photoelectrochemical Properties of Dye-Sensitized Solar Cells Made with Mesoporous TiO <sub>2</sub> Nanoparticles. Journal of Physical Chemistry C, 2008, 112, 8486-8494.	1.5	169
23	Direct Z-Scheme 2D/2D Photocatalyst Based on Ultrathin g-C3N4 and WO3 Nanosheets for Efficient Visible-Light-Driven H2 Generation. ACS Applied Materials & Interfaces, 2019, 11, 27913-27923.	4.0	161
24	Tuning the Valence of the Cerium Center in (Na)phthalocyaninato and Porphyrinato Cerium Double-Deckers by Changing the Nature of the Tetrapyrrole Ligands. Journal of the American Chemical Society, 2003, 125, 12257-12267.	6.6	158
25	Biomimetic Z-scheme photocatalyst with a tandem solid-state electron flow catalyzing H <sub>2</sub> evolution. Journal of Materials Chemistry A, 2018, 6, 15668-15674.	5.2	155
26	Synthesis of anatase TiO2 nanocrystals with {101}, {001} or {010} single facets of 90% level exposure and liquid-phase photocatalytic reduction and oxidation activity orders. Journal of Materials Chemistry A, 2013, 1, 10532.	5.2	147
27	CdS/Regenerated Cellulose Nanocomposite Films for Highly Efficient Photocatalytic H <sub>2</sub> Production under Visible Light Irradiation. Journal of Physical Chemistry C, 2009, 113, 16021-16026.	1.5	143
28	One-pot solvothermal synthesis of MoS2-modified Mn0.2Cd0.8S/MnS heterojunction photocatalysts for highly efficient visible-light-driven H2 production. Applied Catalysis B: Environmental, 2019, 241, 130-140.	10.8	140
29	Pt-loading reverses the photocatalytic activity order of anatase TiO2 {001} and {010} facets for photoreduction of CO2 to CH4. Applied Catalysis B: Environmental, 2014, 144, 855-862.	10.8	138
30	Hydrothermal Preparation of Multiwalled Carbon Nanotubes (MWCNTs)/CdS Nanocomposite and Its Efficient Photocatalytic Hydrogen Production under Visible Light Irradiation. Energy & Fuels, 2011, 25, 2203-2210.	2,5	131
31	Ag-loading on brookite TiO2 quasi nanocubes with exposed {2 1 0} and {0 0 1} facets: Activity and selectivity of CO2 photoreduction to CO/CH4. Applied Catalysis B: Environmental, 2016, 180, 130-138.	10.8	128
32	Selective methanol production from photocatalytic reduction of CO2 on BiVO4 under visible light irradiation. Catalysis Communications, 2012, 28, 38-41.	1.6	127
33	Robust Wide Visible-Light-Responsive Photoactivity for H <sub>2</sub> Production over a Polymer/Polymer Heterojunction Photocatalyst: The Significance of Sacrificial Reagent. ACS Sustainable Chemistry and Engineering, 2015, 3, 1501-1509.	3.2	119
34	Effects of annealing conditions on the photoelectrochemical properties of dye-sensitized solar cells made with ZnO nanoparticles. Solar Energy, 2010, 84, 844-853.	2.9	112
35	Nanometer-sized titanium dioxide micro-column on-line preconcentration of La, Y, Yb, Eu, Dy and their determination by inductively coupled plasma atomic emission spectrometry. Journal of Analytical Atomic Spectrometry, 2001, 16, 863-866.	1.6	109
36	Synthesis of floriated In2S3 decorated with TiO2 nanoparticles for efficient photocatalytic hydrogen production under visible light. Journal of Materials Chemistry, 2011, 21, 14587.	6.7	105

#	Article	IF	CITATIONS
37	Di(alkoxy)- and Di(alkylthio)-Substituted Perylene-3,4;9,10-tetracarboxy Diimides with Tunable Electrochemical and Photophysical Properties. Journal of Organic Chemistry, 2007, 72, 2402-2410.	1.7	104
38	Synthesis of C <sub>60</sub> -decorated SWCNTs (C <sub>60</sub> -d-CNTs) and its TiO <sub>2</sub> -based nanocomposite with enhanced photocatalytic activity for hydrogen production. Dalton Transactions, 2013, 42, 3402-3409.	1.6	101
39	Ti <sub>2</sub> Nb <sub>2x</sub> O <sub>4+5x</sub> anode materials for lithium-ion batteries: a comprehensive review. Journal of Materials Chemistry A, 2018, 6, 9799-9815.	5.2	101
40	Application of TiO <sub>2</sub> Fusiform Nanorods for Dye-Sensitized Solar Cells with Significantly Improved Efficiency. Journal of Physical Chemistry C, 2011, 115, 17213-17219.	1.5	98
41	Controlling the Nature of Mixed (Phthalocyaninato)(porphyrinato) Rare-Earth(III) Double-Decker Complexes: The Effects of Nonperipheral Alkoxy Substitution of the Phthalocyanine Ligand. Chemistry - A European Journal, 2006, 12, 1475-1485.	1.7	90
42	Highly Efficient Photocatalytic Hydrogen Evolution by ReS <sub>2</sub> via a Twoâ€Electron Catalytic Reaction. Advanced Materials, 2018, 30, e1707123.	11.1	90
43	Fundamentals and Recent Progress of Photocatalytic Nitrogenâ€Fixation Reaction over Semiconductors. Solar Rrl, 2021, 5, 2000487.	3.1	90
44	Heteroleptic Bis(Phthalocyaninato) Europium(III) Complexes Fused with Different Numbers of 15-Crown-5 Moieties. Synthesis, Spectroscopy, Electrochemistry, and Supramolecular Structure. Inorganic Chemistry, 2006, 45, 3794-3802.	1.9	88
45	One-pot synthesis of reduced graphene oxide–cadmium sulfide nanocomposite and its photocatalytic hydrogen production. Physical Chemistry Chemical Physics, 2011, 13, 21496.	1.3	88
46	Carbon nitride nanodots decorated brookite TiO2 quasi nanocubes for enhanced activity and selectivity of visible-light-driven CO2 reduction. Applied Catalysis B: Environmental, 2017, 203, 910-916.	10.8	88
47	Visibleâ€Lightâ€Induced Photocatalytic Hydrogen Production over Binuclear Ru <sup>II</sup> –Bipyridyl Dye‣ensitized TiO <sub>2</sub> without Noble Metal Loading. Chemistry - A European Journal, 2012, 18, 12103-12111.	1.7	87
48	High performance organic sensitizers based on 11,12-bis(hexyloxy) dibenzo[a,c]phenazine for dye-sensitized solar cells. Journal of Materials Chemistry, 2012, 22, 18830.	6.7	86
49	Electron-Donating Alkoxy-Group-Driven Synthesis of Heteroleptic Tris(phthalocyaninato) Lanthanide(III) Triple-Deckers with Symmetrical Molecular Structure. Chemistry - A European Journal, 2005, 11, 1425-1432.	1.7	83
50	Triphenylamine-based organic dyes containing a 1,2,3-triazole bridge for dye-sensitized solar cells via a â€ <sup>-</sup> Click' reaction. Dyes and Pigments, 2012, 94, 28-33.	2.0	81
51	New Indole-Based Metal-Free Organic Dyes for Dye-Sensitized Solar Cells. Journal of Physical Chemistry B, 2009, 113, 14588-14595.	1.2	72
52	Hexagonal phase WO3 nanorods: Hydrothermal preparation, formation mechanism and its photocatalytic O2 production under visible-light irradiation. Journal of Solid State Chemistry, 2012, 194, 250-256.	1.4	72
53	Cyclophanes of Perylene Tetracarboxylic Diimide with Different Substituents at Bay Positions. Chemistry - A European Journal, 2008, 14, 7000-7010.	1.7	71
54	Syntheses of asymmetric zinc phthalocyanines as sensitizer of Pt-loaded graphitic carbon nitride for efficient visible/near-IR-light-driven H2 production. Physical Chemistry Chemical Physics, 2014, 16, 4106.	1.3	71

#	Article	IF	CITATIONS
55	Enhanced photocatalytic activity by the construction of a TiO2/carbon nitride nanosheets heterostructure with high surface area via direct interfacial assembly. Nano Research, 2017, 10, 2193-2209.	5.8	71
56	Application of ZnO micro-flowers as scattering layer for ZnO-based dye-sensitized solar cells with enhanced conversion efficiency. Solar Energy, 2014, 101, 150-159.	2.9	70
57	Porphyrin Conjugated Polymer Grafted onto BiVO <sub>4</sub> Nanosheets for Efficient Zâ€5cheme Overall Water Splitting via Cascade Charge Transfer and Singleâ€Atom Catalytic Sites. Advanced Energy Materials, 2021, 11, 2003575.	10.2	70
58	Study of the adsorption behavior ¶of heavy metal ions on nanometer-size ¶titanium dioxide with ICP-AES. Fresenius' Journal of Analytical Chemistry, 2000, 368, 638-640.	1.5	69
59	Synthesis, Characterization, and OFET Properties of Amphiphilic Heteroleptic Tris(phthalocyaninato) Europium(III) Complexes with Hydrophilic Poly(oxyethylene) Substituents. Inorganic Chemistry, 2007, 46, 11397-11404.	1.9	68
60	Bin(Tu)xCl3n: a novel sensitizer and its enhancement of BiOCl nanosheets' photocatalytic activity. Journal of Materials Chemistry, 2012, 22, 8354.	6.7	68
61	A simple preparation method for quasi-solid-state flexible dye-sensitized solar cells by using sea urchin-like anatase TiO2 microspheres. Journal of Power Sources, 2013, 222, 38-44.	4.0	68
62	Efficient Panchromatic Light Harvesting with Co-Sensitization of Zinc Phthalocyanine and Bithiophene-Based Organic Dye for Dye-Sensitized Solar Cells. ACS Sustainable Chemistry and Engineering, 2014, 2, 718-725.	3.2	67
63	Amphiphilic Perylenetretracarboxyl Diimide Dimer and Its Application in Field Effect Transistor. Langmuir, 2007, 23, 5836-5842.	1.6	66
64	Nonperipherally Octa(butyloxy)â€Substituted Phthalocyanine Derivatives with Good Crystallinity: Effects of Metal–Ligand Coordination on the Molecular Structure, Internal Structure, and Dimensions of Selfâ€Assembled Nanostructures. Chemistry - A European Journal, 2009, 15, 13241-13252.	1.7	66
65	Asymmetric Zinc Porphyrin Derivative-Sensitized Graphitic Carbon Nitride for Efficient Visible-Light-Driven H <sub>2</sub> Production. ACS Sustainable Chemistry and Engineering, 2017, 5, 7549-7556.	3.2	66
66	Few-layer BiVO4 nanosheets decorated with SrTiO3: Rh nanoparticles for highly efficient visible-light-driven overall water splitting. Applied Catalysis B: Environmental, 2020, 279, 119377.	10.8	66
67	Hydrothermal synthesis of flaky crystallized La2Ti2O7 for producing hydrogen from photocatalytic water splitting. Catalysis Letters, 2007, 113, 54-58.	1.4	65
68	Synthesis, Structure, Spectroscopic Properties, and Electrochemistry of (1,8,15,22-Tetrasubstituted) Tj ETQq0 0	0 rgBT /O	verlock 10 Tf
69	Effect of Peripheral Hydrophobic Alkoxy Substitution on the Organic Field Effect Transistor Performance of Amphiphilic Tris(phthalocyaninato) Europium Triple-Decker Complexes. Langmuir, 2007, 23, 12549-12554.	1.6	64
70	Carbon encapsulation strategy of Ni co-catalyst: Highly efficient and stable Ni@C/CdS nanocomposite photocatalyst for hydrogen production under visible light. Journal of Catalysis, 2013, 303, 156-163.	3.1	62
71	Efficiently enhanced N2 photofixation performance of sea-urchin-like W18O49 microspheres with Mn-doping. Applied Catalysis B: Environmental, 2019, 254, 351-359.	10.8	60

72New Pyrroleâ€Based Organic Dyes for Dyeâ€Sensitized Solar Cells: Convenient Syntheses and High<br/>Efficiency. Chemistry - A European Journal, 2009, 15, 9664-9668.1.759

#	Article	IF	CITATIONS
73	Fabrication and photoelectrochemical properties of TiO2 films on Ti substrate for flexible dye-sensitized solar cells. Electrochimica Acta, 2010, 55, 5239-5244.	2.6	58
74	Preparation of multiwalled carbon nanotubes/Cd 0.8 Zn 0.2 S nanocomposite and its photocatalytic hydrogen production under visible-light. International Journal of Hydrogen Energy, 2012, 37, 1375-1384.	3.8	58
75	Mg <sub>2</sub> Nb <sub>34</sub> O <sub>87</sub> Porous Microspheres for Use in High-Energy, Safe, Fast-Charging, and Stable Lithium-Ion Batteries. ACS Applied Materials & Interfaces, 2018, 10, 23711-23720.	4.0	58
76	A novel BODIPY-based MOF photocatalyst for efficient visible-light-driven hydrogen evolution. Journal of Materials Chemistry A, 2019, 7, 10439-10445.	5.2	58
77	Synthesis, spectroscopic properties, and electrochemistry of heteroleptic rare earth double-decker complexes with phthalocyaninato and meso-tetrakis (4-chlorophenyl)porphyrinato ligands. New Journal of Chemistry, 2004, 28, 1116-1122.	1.4	57
78	Ru(II) complexes bearing 2,6-bis(benzimidazole-2-yl)pyridine ligands: A new class of catalysts for efficient dehydrogenation of primary alcohols to carboxylic acids and H2 in the alcohol/CsOH system. Journal of Organometallic Chemistry, 2017, 830, 11-18.	0.8	57
79	Studies of "Pinwheel-Like―Bis[1,8,15,22-tetrakis(3-pentyloxy)phthalocyaninato] Rare Earth(III) Double-Decker Complexes. Chemistry - A European Journal, 2005, 11, 7351-7357.	1.7	56
80	MoS2-MoO3-x hybrid cocatalyst for effectively enhanced H2 production photoactivity of AgIn5S8 nano-octahedrons. Applied Catalysis B: Environmental, 2018, 228, 39-46.	10.8	55
81	Enhanced Energy Conversion Efficiency of Mg <sup>2+</sup> -Modified Mesoporous TiO <sub>2</sub> Nanoparticles Electrodes for Dye-Sensitized Solar Cells. Journal of Physical Chemistry C, 2010, 114, 22346-22351.	1.5	52
82	Asymmetric zinc porphyrin-sensitized nanosized TiO <sub>2</sub> for efficient visible-light-driven CO <sub>2</sub> photoreduction to CO/CH <sub>4</sub> . Chemical Communications, 2015, 51, 12443-12446.	2.2	52
83	Highly efficient visible/near-IR-light-driven photocatalytic H2 production over asymmetric phthalocyanine-sensitized TiO2. RSC Advances, 2013, 3, 14363.	1.7	50
84	Porphyrin-Based Metal–Organic Frameworks for Efficient Photocatalytic H <sub>2</sub> Production under Visible-Light Irradiation. Inorganic Chemistry, 2021, 60, 3988-3995.	1.9	49
85	Effects of rare earth ion modifications on the photoelectrochemical properties of ZnO-based dye-sensitized solar cells. Renewable Energy, 2011, 36, 3386-3393.	4.3	48
86	Preparation of brookite titania quasi nanocubes and their application in dye-sensitized solar cells. Journal of Materials Chemistry A, 2015, 3, 7453-7462.	5.2	46
87	Synthesis and Characterization of Mixed Phthalocyaninato andmeso-Tetrakis(4-chlorophenyl)porphyrinato Triple-Decker Complexesâ^' Revealing the Origin of Their Electronic Absorptions. European Journal of Inorganic Chemistry, 2004, 2004, 3806-3813.	1.0	45
88	Synthesis of multicomponent sulfide Ag <sub>2</sub> ZnSnS <sub>4</sub> as an efficient photocatalyst for H <sub>2</sub> production under visible light irradiation. RSC Advances, 2013, 3, 253-258.	1.7	45
89	Airâ€stable Ruthenium(II)â€NNN Pincer Complexes for the Efficient Coupling of Aromatic Diamines and Alcohols to 1 <i>H</i> â€benzo[ <i>d</i> ]imidazoles with the Liberation of H <sub>2</sub> . ChemCatChem, 2018, 10, 1607-1613.	1.8	45
90	Synthesis, Structure, and Spectroscopic and Electrochemical Properties of Heteroleptic Bis(phthalocyaninato) Rare Earth Complexes with aC4 Symmetry. Helvetica Chimica Acta, 2004, 87, 2581-2596.	1.0	44

#	Article	IF	CITATIONS
91	Construction of inorganic nanoparticles by micro-nano-porous structure of cellulose matrix. Cellulose, 2011, 18, 945-956.	2.4	44
92	Rice-like brookite titania as an efficient scattering layer for nanosized anatase titania film-based dye-sensitized solar cells. Journal of Power Sources, 2014, 260, 233-242.	4.0	44
93	Porphyrin Conjugated Polymer with Periodic Type IIâ€Like Heterojunctions and Singleâ€Atom Catalytic Sites for Broadbandâ€Responsive Hydrogen Evolution. Advanced Functional Materials, 2021, 31, 2009819.	7.8	44
94	Preparation of Single-Crystalline AgIn <sub>5</sub> S <sub>8</sub> Octahedrons with Exposed {111} Facets and Its Visible-Light-Responsive Photocatalytic H <sub>2</sub> Production Activity. ACS Applied Materials & Interfaces, 2017, 9, 17013-17023.	4.0	43
95	Controllable Fabrication of Regular Hexagon-Shaped SnS <sub>2</sub> Nanoplates and Their Enhanced Visible-Light-Driven H <sub>2</sub> Production Activity. ACS Applied Nano Materials, 2018, 1, 2923-2933.	2.4	43
96	Lanthanide(III) Double-Decker Complexes with Octaphenoxy- or Octathiophenoxyphthalocyaninato Ligands – Revealing the Electron-Withdrawing Nature of the Phenoxy and Thiophenoxy Groups in the Double-Decker Complexes. European Journal of Inorganic Chemistry, 2006, 2006, 3703-3709.	1.0	42
97	Enhanced photodegradation efficiency of polyethyleneâ€īiO <sub>2</sub> nanocomposite film with oxidized polyethylene wax. Journal of Applied Polymer Science, 2010, 118, 378-384.	1.3	42
98	Influence of different ruthenium(II) bipyridyl complex on the photocatalytic H2 evolution over TiO2 nanoparticles with mesostructures. Journal of Power Sources, 2008, 180, 498-505.	4.0	41
99	Iodine-free quasi solid-state dye-sensitized solar cells based on ionic liquid and alkali salt. Journal of Materials Chemistry, 2011, 21, 16448.	6.7	41
100	Porphyrin-Based Conjugated Polymers as Intrinsic Semiconducting Photocatalysts for Robust H <sub>2</sub> Generation under Visible Light. ACS Applied Energy Materials, 2019, 2, 5665-5676.	2.5	39
101	Synthetic, Structural, Spectroscopic, and Electrochemical Studies of Heteroleptic Tris(phthalocyaninato) Rare Earth Complexes. European Journal of Inorganic Chemistry, 2005, 2005, 2612-2618.	1.0	38
102	Ni( <scp>ii</scp> )–N′NN′ pincer complexes catalyzed dehydrogenation of primary alcohols to carboxylic acids and H <sub>2</sub> accompanied by alcohol etherification. Catalysis Science and Technology, 2017, 7, 2506-2511.	2.1	38
103	An efficient copper phthalocyanine additive of perovskite precursor for improving the photovoltaic performance of planar perovskite solar cells. Journal of Power Sources, 2017, 359, 303-310.	4.0	38
104	Synthesis of size controllable and thermally stable rice-like brookite titania and its application as a scattering layer for nano-sized titania film-based dye-sensitized solar cells. Journal of Materials Chemistry A, 2014, 2, 1886-1896.	5.2	37
105	Layered WS2/WO3 Z-scheme photocatalyst constructed via an in situ sulfurization of hydrous WO3 nanoplates for efficient H2 generation. Applied Surface Science, 2020, 529, 147013.	3.1	37
106	Hydrothermal fabrication of PbMoO4 microcrystals with exposed (001) facets and its enhanced photocatalytic properties. CrystEngComm, 2011, 13, 2785.	1.3	36
107	Syntheses of asymmetric zinc porphyrins bearing different pseudo-pyridine substituents and their photosensitization for visible-light-driven H <sub>2</sub> production activity. Dalton Transactions, 2017, 46, 8219-8228.	1.6	36
108	Heteroleptic Rare Earth Double-Decker Complexes with Naphthalocyaninato and Phthalocyaninato Ligands. General Synthesis, Spectroscopic, and Electrochemical Characteristics. Inorganic Chemistry, 2005, 44, 2114-2120.	1.9	35

#	Article	IF	CITATIONS
109	A new route for visible/near-infrared-light-driven H2 production over titania: Co-sensitization of surface charge transfer complex and zinc phthalocyanine. Journal of Power Sources, 2015, 298, 30-37.	4.0	35
110	Homoleptic Lanthanide Triple-Deckers of 5,15-Diazaporphyrin withD2hSymmetry. Inorganic Chemistry, 2004, 43, 8242-8244.	1.9	34
111	Effects of tetrabutoxytitanium on photoelectrochemical properties of plastic-based TiO2 film electrodes for flexible dye-sensitized solar cells. Journal of Power Sources, 2011, 196, 2939-2944.	4.0	34
112	A new class of organic dyes containing β-substituted 2, 2′-bithiophenene unit as a π-linker for dye-sensitized solar cells: Structural modification for understanding relationship of structure and photovoltaic performances. Journal of Power Sources, 2013, 234, 23-30.	4.0	34
113	One-pot hydrothermal synthesis of MoS <sub>2</sub> -modified Mn <sub>0.5</sub> Cd <sub>0.5</sub> S solid solution for boosting H <sub>2</sub> production activity under visible light. Catalysis Science and Technology, 2019, 9, 762-771.	2.1	33
114	Asymmetry and electronic directionality: a means of improving the red/near-IR-light-responsive photoactivity of phthalocyanine-sensitized carbon nitride. Catalysis Science and Technology, 2014, 4, 3251.	2.1	32
115	Highly Asymmetric Tribenzonaphthoâ€Condensed Porphyrazinatozinc Complex: An Efficient Nearâ€Infrared Sensitizer for Dyeâ€Sensitized Solar Cells. ChemPlusChem, 2012, 77, 1022-1027.	1.3	31
116	Central site regulation of cobalt porphyrin conjugated polymer to give highly active and selective CO2 reduction to CO in aqueous solution. Applied Catalysis B: Environmental, 2021, 291, 120128.	10.8	31
117	Walnut-like In2S3 microspheres: ionic liquid-assisted solvothermal synthesis, characterization and formation mechanism. Nanoscale, 2012, 4, 2372.	2.8	30
118	Effects of benzo-annelation of asymmetric phthalocyanine on the photovoltaic performance of dye-sensitized solar cells. Dalton Transactions, 2014, 43, 8421-8430.	1.6	30
119	Ruâ€Pincer Complexâ€Bridged Cuâ€Porphyrin Polymer for Robust (Photo)Electrocatalytic H <sub>2</sub> Evolution via Singleâ€Atom Active Sites. Advanced Functional Materials, 2021, 31, 2107290.	7.8	30
120	Preparation of brookite TiO <sub>2</sub> nanoparticles with small sizes and the improved photovoltaic performance of brookite-based dye-sensitized solar cells. Nanoscale, 2016, 8, 18771-18781.	2.8	29
121	Synthesis of an A2BC-type asymmetric zinc phthalocyanine derivative for efficient visible/near-infrared-driven H2 evolution on g-C3N4. Chemical Engineering Journal, 2019, 373, 651-659.	6.6	29
122	Effects of the central metal ions on the photosensitization of metalloporphyrins over carbon nitride for visible-light-responsive H2 production. Applied Surface Science, 2019, 464, 255-261.	3.1	29
123	Facile Preparation Process of NiCoP–NiCoSe <sub>2</sub> Nano-Bilayer Films for Oxygen Evolution Reaction with High Efficiency and Long Duration. ACS Sustainable Chemistry and Engineering, 2020, 8, 1240-1251.	3.2	29
124	New organic dyes containing tert-Butyl-capped N-Arylcarbazole moiety for Dye-sensitized solar cells. RSC Advances, 2012, 2, 7081.	1.7	28
125	Oxidant-free synthesis of benzimidazoles from alcohols and aromatic diamines catalysed by new Ru( <scp>ii</scp> )-PNS(O) pincer complexes. Dalton Transactions, 2017, 46, 15012-15022.	1.6	28
126	Oneâ€Pot Synthesis of Cuâ€Nanoclusterâ€Decorated Brookite TiO <sub>2</sub> <i>Quasi</i> â€Nanocubes for Enhanced Activity and Selectivity of CO <sub>2</sub> Photoreduction to CH <sub>4</sub> . ChemPhysChem, 2017, 18, 3230-3239.	1.0	28

#	Article	IF	CITATIONS
127	Self-organized film of ultra-fine TiO2 nanotubes and its application to dye-sensitized solar cells on a flexible Ti-foil substrate. Journal of Materials Chemistry, 2012, 22, 4681.	6.7	27
128	SrCO3-modified brookite/anatase TiO2 heterophase junctions with enhanced activity and selectivity of CO2 photoreduction to CH4. Applied Surface Science, 2019, 476, 937-947.	3.1	27
129	Bis[1,4,8,11,15,18,22,25-octa(butyloxyl)phthalocyaninato] rare earth double-decker complexes: synthesis, spectroscopy, and molecular structure. Dalton Transactions, 2010, 39, 1321-1327.	1.6	26
130	Synthesis and characterization of an A2BC type phthalocyanine and its visible-light-responsive photocatalytic H2 production performance on graphitic carbon nitride. Dalton Transactions, 2016, 45, 14071-14079.	1.6	26
131	Controllable Preparation of Rutile TiO <sub>2</sub> Nanorod Array for Enhanced Photovoltaic Performance of Perovskite Solar Cells. ACS Applied Energy Materials, 2018, 1, 1649-1657.	2.5	26
132	New Ru( <scp>ii</scp> ) N′NN′-type pincer complexes: synthesis, characterization and the catalytic hydrogenation of CO <sub>2</sub> or bicarbonates to formate salts. New Journal of Chemistry, 2017, 41, 3055-3060.	1.4	25
133	In-situ growth of ultrafine ZnO on g-C3N4 layer for highly active and selective CO2 photoreduction to CH4 under visible light. Materials Research Bulletin, 2021, 137, 111177.	2.7	25
134	A novel preparation of small TiO2 nanoparticle and its application to dye-sensitized solar cells with binder-free paste at low temperature. Nanoscale, 2011, 3, 3900.	2.8	24
135	Low-temperature preparation of AgIn5S8/TiO2 heterojunction nanocomposite with efficient visible-light-driven hydrogen production. International Journal of Hydrogen Energy, 2013, 38, 15965-15975.	3.8	24
136	Hierarchical PbMoO4microspheres: hydrothermal synthesis, formation mechanism and photocatalytic properties. CrystEngComm, 2013, 15, 1146-1152.	1.3	24
137	Low-cost, quasi-solid-state and TCO-free highly bendable dye-sensitized cells on paper substrate. Journal of Materials Chemistry, 2012, 22, 16121.	6.7	23
138	Construction of Ag <sub>2</sub> S/WO <sub>3</sub> Direct Z-Scheme Photocatalyst for Enhanced Charge Separation Efficiency and H <sub>2</sub> Generation Activity. Industrial & Engineering Chemistry Research, 2019, 58, 14802-14813.	1.8	23
139	Effects of the symmetry and carboxyl anchoring group of zinc phthalocyanine derivatives on g-C <sub>3</sub> N <sub>4</sub> for photosensitized H <sub>2</sub> production. RSC Advances, 2016, 6, 77366-77374.	1.7	22
140	Electronâ€Rich Pincer Ligand oupled Cobalt Porphyrin Polymer with Singleâ€Atom Sites for Efficient (Photo)Electrocatalytic CO <sub>2</sub> Reduction at Ultralow Overpotential. Small, 2021, 17, e2102957.	5.2	22
141	Insight into the significantly enhanced photocatalytic CO2 reduction performance of Pt/MnO dual cocatalysts on sea-urchin-like anatase TiO2 microspheres. Chemical Engineering Journal, 2021, 425, 131627.	6.6	22
142	Recent Development of Dye-Sensitized Solar Cells Based on Flexible Substrates. Science of Advanced Materials, 2013, 5, 1596-1626.	0.1	22
143	Synthesis, characterization of CdS/rectorite nanocomposites and its photocatalytic activity. Physics and Chemistry of Minerals, 2007, 34, 275-285.	0.3	21
144	Sandwichâ€Type Heteroleptic <i>opposite</i> â€(Diazaporphyrinato)cerium Complexes: Synthesis, Spectroscopy, Structure, and Electrochemistry. European Journal of Inorganic Chemistry, 2008, 2008, 5519-5523.	1.0	21

#	Article	IF	CITATIONS
145	Composite electrode of TiO <sub>2</sub> particles with different crystal phases and morphology to significantly improve the performance of dye-sensitized solar cells. RSC Advances, 2015, 5, 32536-32545.	1.7	21
146	Low cost and solution-processable zinc phthalocyanine as alternative hole transport material for perovskite solar cells. RSC Advances, 2016, 6, 107723-107731.	1.7	21
147	Photosensitization of zinc phthalocyanine bearing 15-crown-5 ether moieties on carbon nitride for H2 production: Effect of co-existing alkali metal ions. Journal of Power Sources, 2018, 396, 57-63.	4.0	21
148	Enhancement of photocatalytic degradation of poly(vinyl chloride) with perchlorinated iron (II) phthalocyanine modified nanoâ€₹iO <sub>2</sub> . Journal of Applied Polymer Science, 2011, 122, 1823-1828.	1.3	20
149	Fabrication of an Feâ€Doped SrTiO <sub>3</sub> Photocatalyst with Enhanced Dinitrogen Photofixation Performance. European Journal of Inorganic Chemistry, 2019, 2019, 2182-2192.	1.0	20
150	Z-scheme photocatalyst based on porphyrin derivative decorated few-layer BiVO4 nanosheets for efficient visible-light-driven overall water splitting. Nano Research, 2021, 14, 1294-1304.	5.8	20
151	Asymmetric zinc phthalocyanines with large steric hindrance as efficient red/near-IR responsive sensitizer for dye-sensitized solar cells. Dyes and Pigments, 2015, 114, 231-238.	2.0	19
152	Controllable Syntheses of Hierarchical WO <sub>3</sub> Films Consisting of Orientation-Ordered Nanorod Bundles and Their Photocatalytic Properties. Crystal Growth and Design, 2018, 18, 794-801.	1.4	19
153	Divalent Manganese Linked Tungstenâ^'Molybdenum Polyoxometalates:  Synthesis, Structure, and Magnetic Characteristics. Crystal Growth and Design, 2007, 7, 1699-1705.	1.4	18
154	Enhancement of photocatalytic degradation activity of poly(vinyl chloride)â€TiO <sub>2</sub> nanocomposite film with polyoxometalate. Journal of Applied Polymer Science, 2011, 120, 2048-2053.	1.3	18
155	Preparation of Ni@C–Cd <sub>0.8</sub> Zn <sub>0.2</sub> S nanocomposites with highly efficient and stable photocatalytic hydrogen production activity. Physical Chemistry Chemical Physics, 2015, 17, 10944-10952.	1.3	18
156	Lowâ€Temperature Processed Nanostructured Rutile TiO <sub>2</sub> Array Films for Perovskite Solar Cells With High Efficiency and Stability. Solar Rrl, 2018, 2, 1700164.	3.1	18
157	Synthesis of zinc phthalocyanine with large steric hindrance and its photovoltaic performance for dye-sensitized solar cells. Dalton Transactions, 2015, 44, 5867-5874.	1.6	17
158	Effect of carboxyl anchoring groups in asymmetric zinc phthalocyanine with large steric hindrance on the dye-sensitized solar cell performance. Materials Chemistry and Physics, 2015, 163, 348-354.	2.0	17
159	Separation/Preconcentration of Lanthanum and Europium by Micro-Column Packed with Immobilized 1-Phenyl-3-methyl-4-bonzoyl-5-pyrazone on Microcrystalline Naphthalene and Determination by Electrothermal Vaporization Inductively Coupled Plasma-Atomic Emission Spectrometry Analytical Sciences. 1999. 15, 737-741.	0.8	16
160	Highly asymmetric phthalocyanine-sensitized solar cells: The effect of coadsorbent and adsorption temperature of phthalocyanine. Electrochimica Acta, 2013, 111, 344-350.	2.6	16
161	Optimization of plastic crystal ionic liquid electrolyte for solid-state dye-sensitized solar cell. Electrochimica Acta, 2013, 94, 1-6.	2.6	16
162	Bilayer film electrode of brookite TiO2 particles with different morphology to improve the performance of pure brookite-based dye-sensitized solar cells. Journal of Power Sources, 2016, 327, 77-85.	4.0	16

#	Article	IF	CITATIONS
163	Co-porphyrin/Ru-pincer complex coupled polymer with Z-scheme molecular junctions and dual single-atom sites for visible light-responsive CO2 reduction. Chemical Engineering Journal, 2022, 431, 133357.	6.6	16
164	Study on the direct analysis of solid powder biological samples using fluorination assisted electrothermal vaporization inductively coupled plasma atomic emission spectrometry with PTFE slurry modifier. Fresenius' Journal of Analytical Chemistry, 1999, 364, 556-559.	1.5	15
165	H <sub>2</sub> O-Involved Hydrogen Bonds in Pseudo-Double-Decker Supramolecular Structure of 1,8,15,22-Tetrasubstituted Phthalocyaninato Zinc Complex. Crystal Growth and Design, 2008, 8, 4454-4459.	1.4	15
166	Fabrication of alumina nanofibers by precipitation reaction combined with heterogeneous azeotropic distillation process. Materials Research Bulletin, 2009, 44, 160-167.	2.7	15
167	A novel Cul-based iodine-free gel electrolyte for dye-sensitized solar cells. Electrochimica Acta, 2011, 56, 5554-5560.	2.6	15
168	An efficient binary ionic liquid based quasi solid-state electrolyte for dye-sensitized solar cells. Electrochimica Acta, 2013, 107, 231-237.	2.6	15
169	Review of Z-Scheme Heterojunctions for Photocatalytic Energy Conversion. Wuli Huaxue Xuebao/ Acta Physico - Chimica Sinica, 2020, .	2.2	15
170	Slurry sampling fluorination assisted electrothermal vaporization-inductively coupled plasma-atomic emission spectrometry for the direct determination of metal impurities in aluminium oxide ceramic powders. Fresenius' Journal of Analytical Chemistry, 2001, 369, 461-465.	1.5	14
171	Single-crystal β-MnO2 hollow bipyramids: synthesis and application in lithium ion batteries. RSC Advances, 2013, 3, 5141.	1.7	14
172	Multiwalled Carbon Nanotube-TiO <sub>2</sub> Nanocomposite for Visible-Light-Induced Photocatalytic Hydrogen Evolution. Journal of Nanomaterials, 2014, 2014, 1-8.	1.5	14
173	Synthesis of asymmetric zinc phthalocyanine with bulky diphenylthiophenol substituents and its photovoltaic performance for dye-sensitized solar cells. Journal of Photochemistry and Photobiology A: Chemistry, 2016, 321, 248-256.	2.0	14
174	Brookite TiO <sub>2</sub> Nanoparticles Decorated with Ag/MnO <sub><i>x</i></sub> Dual Cocatalysts for Remarkably Boosted Photocatalytic Performance of the CO <sub>2</sub> Reduction Reaction. Langmuir, 2021, 37, 12487-12500.	1.6	14
175	Direct ICP-AES Determination of Trace Impurities in Silicon Dioxide Using Fluorinating Electrothermal Vaporization with Slurry Sampling Analytical Sciences, 1997, 13, 595-599.	0.8	12
176	Direct determination of trace copper and chromium in silicon nitride by fluorinating electrothermal vaporization inductively coupled plasma atomic emission spectrometry with the slurry sampling technique. Fresenius' Journal of Analytical Chemistry, 1999, 364, 551-555.	1.5	12
177	In-situ separation of chromium(III) and chromium(VI) and sequential ETV-ICP-AES determination using acetylacetone and PTFE as chemical modifiers. Fresenius' Journal of Analytical Chemistry, 2001, 370, 904-908.	1.5	12
178	The effect of Mg doping on the dielectric and tunable properties of Pb0.3Sr0.7TiO3 thin films prepared by sol–gel method. Applied Physics A: Materials Science and Processing, 2014, 114, 777-783.	1.1	12
179	Investigation of benzo(1,2-b:4,5-b′)dithiophene as a spacer in organic dyes for high efficient dye-sensitized solar cell. Organic Electronics, 2015, 25, 245-253.	1.4	11
180	Growth of a sea urchin-like rutile TiO <sub>2</sub> hierarchical microsphere film on Ti foil for a quasi-solid-state dye-sensitized solar cell. Nanoscale, 2017, 9, 18498-18506.	2.8	11

#	Article	IF	CITATIONS
181	In situ grown TiN/N-TiO2 composite for enhanced photocatalytic H2 evolution activity. Frontiers in Energy, 2021, 15, 721-731.	1.2	11
182	Monoclinic WO3 nanosheets-carbon nanotubes nanocomposite based electrochemical sensor for sensitive detection of bisphenol A. Journal of Electroanalytical Chemistry, 2022, 915, 116355.	1.9	11
183	Direct analysis of silicon carbide by fluorination assisted electrothermal vaporization inductively coupled plasma atomic emission spectrometry using a slurry sampling technique. Analyst, The, 2000, 125, 2089-2093.	1.7	10
184	The molecular, electronic structures and vibrational spectra of metal-free, N,N′-dideuterio and magnesium tetra-2,3-pyridino-porphyrazines: Density functional calculations. Spectrochimica Acta - Part A: Molecular and Biomolecular Spectroscopy, 2006, 65, 467-480.	2.0	10
185	New anthracene-based organic dyes: the flexible position of the anthracene moiety bearing isolation groups in the conjugated bridge and the adjustable cell performance. Organic Chemistry Frontiers, 2016, 3, 233-242.	2.3	10
186	Electrochemistry of homoleptic bis[3(4),12(13),21(22),30(31)-tetra( <i>tert</i> -butyl)-naphthalocyaninato] rare earth(III) complexes. Journal of Porphyrins and Phthalocyanines, 2005, 09, 40-46.	0.4	9
187	Benzo-fused low symmetry metal-free tetraazaporphyrin and phthalocyanine analogs: synthesis, spectroscopy, electrochemistry, and density functional theory calculations. Journal of Porphyrins and Phthalocyanines, 2010, 14, 421-437.	0.4	9
188	Low Dielectric Loss and Good Dielectric Thermal Stability of <i>xx</i> <scp><scp>Nd</scp></scp> ( <scp>Zn</scp> <sub>1/2</sub> <scp><scp>Ti</scp></scp> Thin Films Fabricated by Sol–Gel Method. Journal of the American Ceramic Society, 2013, 96, 820-824.	5 <b>1.b</b> /2 <td>o9)<scp><so< td=""></so<></scp></td>	o9) <scp><so< td=""></so<></scp>
189	Ruthenium(II) Pincer Complex Bearing N′NN′―and ONOâ€Type Ligands as a Titania Sensitizer for Efficient and Stable Visibleâ€Lightâ€Driven Hydrogen Production. ChemPhotoChem, 2018, 2, 765-772.	1.5	9
190	Efficient CO <sub>2</sub> reduction over a Ru-pincer complex/TiO <sub>2</sub> hybrid photocatalyst <i>via</i> direct Z-scheme mechanism. Catalysis Science and Technology, 2022, 12, 1637-1650.	2.1	8
191	Sea urchin-like TiO2 microspheres as scattering layer of nanosized TiO2 film-based dye-sensitized solar cell with enhanced conversion efficiency. Materials Chemistry and Physics, 2015, 164, 238-245.	2.0	7
192	Improved photovoltaic performance of perovskite solar cells based on three-dimensional rutile TiO <sub>2</sub> nanodendrite array film. Nanoscale, 2018, 10, 20836-20843.	2.8	7
193	Effect of electron-withdrawing groups in conjugated bridges: molecular engineering of organic sensitizers for dye-sensitized solar cells. Frontiers of Optoelectronics, 2016, 9, 60-70.	1.9	6
194	Theoretical investigation of self-assembled donor–acceptor phthalocyanine complexes and their application in dye-sensitized solar cells. Journal of Molecular Graphics and Modelling, 2015, 59, 100-106.	1.3	5
195	Asymmetric zinc porphyrin derivatives bearing three pseudo-pyrimidine meso-position substituents and their photosensitization for H2 evolution. New Journal of Chemistry, 2020, 44, 11237-11247.	1.4	5
196	In-situ Separation of a Matrix for the Direct Analysis of Zirconium Dioxide Powder by Electrothermal Vaporization ICP-AES with a Polytetrafluoroethylene Slurry Modifier Analytical Sciences, 2000, 16, 877-879.	0.8	4
197	Linear perylenetetracarboxylic monoanhydried derivatives for the sensitization of dye-sensitized solar cells. Journal of Photochemistry and Photobiology A: Chemistry, 2012, 239, 28-36.	2.0	3
198	New Ni(II) complexes based on N′NN′ pincer ligands: syntheses, structures and B–F cleavage of BF <sub>4</sub> <sup>â²'</sup> promoted by a di-cationic Ni(II) center. Journal of Coordination Chemistry, 2016, 69, 2353-2363.	0.8	3

#	Article	IF	CITATIONS
199	TiO <sub>2</sub> modified with a Ru( <scp>ii</scp> )–N′NN′ 8-hydroxyquinolyl complex for efficient gaseous photoreduction of CO <sub>2</sub> . Catalysis Science and Technology, 2018, 8, 2098-2103.	2.1	3
200	4,5-Bis(4-methoxyphenoxy)phthalonitrile. Acta Crystallographica Section E: Structure Reports Online, 2010, 66, o2527-o2527.	0.2	2
201	Preparation of a Single-Walled Carbon Nanotube/Cd0.8Zn0.2S Nanocomposite and Its Enhanced Photocatalytic Hydrogen Production Activity. European Journal of Inorganic Chemistry, 2016, 2016, 3204-3212.	1.0	2
202	Solution-Processable Cu(II) Phthalocyanine Derivative as Dopant-Free Hole Transport Layer for Efficient and Low-Cost Rutile TiO <sub>2</sub> Array-Based Perovskite Solar Cells. ACS Applied Energy Materials, 0, , .	2.5	2
203	An effective Z-scheme hybrid photocatalyst based on zinc porphyrin derivative and anatase titanium dioxide microsphere for carbon dioxide reduction. Materials Today Sustainability, 2022, 19, 100164.	1.9	2
204	1,3-Dimethyl-5,6,7,8-tetrahydro-4H-cyclohepta[c]thiophene-4,8-dione. Acta Crystallographica Section E: Structure Reports Online, 2010, 66, o3231-o3231.	0.2	1
205	Effects of Metal Oxide Modifications on Photoelectrochemical Properties of Mesoporous TiO2 Nanoparticles Electrodes for Dye-Sensitized Solar Cells. Chinese Journal of Chemical Physics, 2012, 25, 609-616.	0.6	1
206	Synthesis and electrochemical properties of FeSbO4 nanorods. Wuhan University Journal of Natural Sciences, 2013, 18, 185-190.	0.2	1
207	New Progress in Monomeric Phthalocyanine Chemistry: Synthesis, Crystal Structures and Properties. Structure and Bonding, 2009, , 121-160.	1.0	1